CHAPTER 8

Summary and Future Scope

8.1 Summary

This final chapter presents an overview of the thesis, highlighting the key findings obtained from various investigations. The present research focuses on the development of heterostructure photocatalysts for efficient H_2O_2 production and *in-situ* utilization for antibiotic degradation.

This research work fabricated 2D $MoS_2/MnIn_2S_4$, $Ag/NiFe_2O_4/CuWO_4$, Ag/s-($Co_3O_4/NiFe_2O_4$), Ag loaded starch functionalized-Fe_3O_4, and Ag loaded starch functionalized-Fe_3O_4/AgI photocatalytic systems. The preparation of these photocatalysts followed a stepwise hydrothermal and precipitation preparation protocol. XRD investigated the phase formation, TEM images identified heterostructure formation in photocatalyst particles, while XPS was used to identify the chemical elements constituting the composite and their oxidation states. A large-scale classical MD simulation investigated the oxygen and water adsorption affinity towards respective semiconductor components. The component bandgaps, band positions, and recombination issues were investigated by UV–visible diffuse reflectance spectroscopy (UV-DRS), Mott-Schottky, and photoluminescence studies on as-prepared samples. The adsorption property of photocatalysts was observed by measuring the contact angle. Extensive control experiments helped gain insight into the operating photocatalytic mechanism.

Chapter 3 of the thesis presents the development of ultrathin 2D MoS_2 nanosheets embedded with $MnIn_2S_4$ heterostructure photocatalysts for efficient solar-driven H_2O_2 production. Optimal $MnIn_2S_4$ loading enhances light absorption and charge separation by partially covering MoS_2, while excessive loading hinders performance by blocking active sites. The superior photocatalytic performance, about 3.3 times higher than physically mixed counterparts, highlights the importance of intimate interfacial contact in the

heterostructure for effective charge transfer and recombination suppression. Microscopy confirms strong interfacial interactions between the parts of the composite. Radical trapping studies reveal that H_2O_2 is generated via a dual-step, one-electron O_2 reduction pathway.

Chapters 4, 5, 6, and 7 of this research focus on the development and photocatalytic performance of Ag/$CuWO_4$/$NiFe_2O_4$, Ag/s-(Co_3O_4/$NiFe_2O_4$), Ag-loaded starch functionalized-Fe_3O_4, and Ag-loaded starch functionalized-Fe_3O_4/AgI, magnetic recyclable visible light photocatalytic systems for H_2O_2 production under various conditions. The incorporation of Ag significantly enhances photocatalytic H_2O_2 generation by promoting the direct two-electron O_2 reduction pathway, improving visible-light absorption, and facilitating charge transfer. Moreover, Ag increases the O_2 adsorption affinity on the photocatalyst surface. Furthermore, the H_2O_2 produced by this process could efficiently degrade tetracycline.

Figure 8.1 presents a comparative analysis of photocatalytic H_2O_2 production achieved in this study alongside recently reported photocatalysts under pure water conditions. Notably, the Ag/s-(Co_3O_4/$NiFe_2O_4$), Ag-loaded starch-functionalized Fe_3O_4 (ASM), and Ag-loaded starch-functionalized Fe_3O_4/AgI (10ASM/AgI) demonstrated efficient H_2O_2 generation without the use of sacrificial agents or external O_2 purging. These findings demonstrate the critical role of surface modification in enhancing photocatalytic activity. Starch functionalization significantly improves the hydrophilicity of the photocatalyst surface, which facilitates water oxidation by increasing the residence time of water molecules near the catalyst surface. This prolonged interaction between water molecules and the active sites of Ag/s-(Co_3O_4/$NiFe_2O_4$), ASM, and 10ASM/AgI enhances their interaction with both the catalyst and reactant species. Among these systems, the

photocatalyst designed in this study exhibits superior H_2O_2 production activity in pure water compared to the recently reported counterparts (Table 8.1). This advancement highlights the potential for efficient, sacrificial agent-free photocatalytic H_2O_2 production under environmentally benign conditions.

Table 8.1 Comparison of photocatalytic H_2O_2 generation over recently reported photocatalysts using pure water.

Photocatalysts	**Reaction condition**	**Light Source**	**H_2O_2 production ($\mu mol\ h^{-1}\ g^{-1}$)**	**Ref.**
ZnPPc-NBCN	Only water	$\lambda > 420$ nm	114 $\mu mol\ h^{-1}\ g^{-1}$	[251]
PI/$ZnIn_2S_4$	Only water	$\lambda > 420$ nm	411.07	[252]
TZ-COF	Only water	$\lambda > 420$ nm	268 $\mu mol\ h^{-1}\ g^{-1}$	[253]
OZ-COF	Only water	$\lambda > 420$ nm	220 $\mu mol\ h^{-1}\ g^{-1}$	[253]
IZ-COF	Only water	$\lambda > 420$ nm	102 $\mu mol\ h^{-1}\ g^{-1}$	[253]
COF-N32	Only water	$\lambda > 420$ nm	605 $\mu mol\ h^{-1}\ g^{-1}$	[254]
COF-N33	Only water	$\lambda > 420$ nm	155 $\mu mol\ h^{-1}\ g^{-1}$	[254]
g-C_3N_4/Co_9S_8	Only water	$\lambda > 420$ nm	826 $\mu mol\ h^{-1}\ g^{-1}$	[255]
Pt/KCN	Only water	250 W Na lamp ($400 < \lambda < 800$ nm)	155 $\mu mol\ h^{-1}\ g^{-1}$	[42]
Ag/s-(Co_3O_4/$NiFe_2O_4$)	Only water	Cool white LED	1250 $\mu mol\ h^{-1}\ g^{-1}$	Chapter 5
10ASM	Only water	Cool white LED	258.7 $\mu mol\ h^{-1}\ g^{-1}$	Chapter 6
10ASM/AgI	Only water	Cool white LED	891 $\mu mol\ h^{-1}\ g^{-1}$	Chapter 7

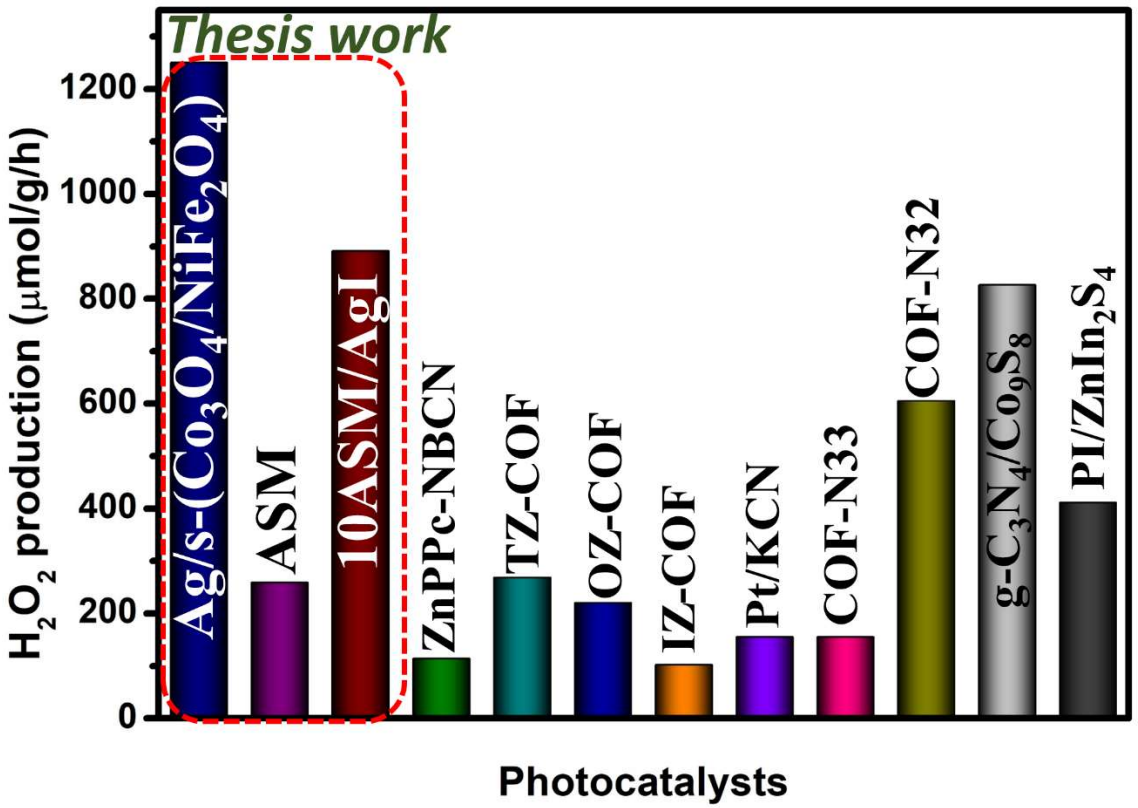

Figure 8.1. Comparison of the photocatalytic H_2O_2 production of this thesis work with recently reported photocatalysts under pure water conditions.

In addition, Figure 8.2 presents a comparative analysis of photocatalytic H_2O_2 production achieved in this study alongside recently reported heterostructure photocatalysts in water with O_2 purging conditions. All the designed heterostructure photocatalysts-2D $MoS_2/MnIn_2S_4$, $Ag/CuWO_4/NiFe_2O_4$, Ag/s-(Co_3O_4/$NiFe_2O_4$), ASM, and 10ASM/AgI-exhibited considerable H_2O_2 production under these conditions. Among them, Ag/s-(Co_3O_4/$NiFe_2O_4$) and 10ASM/AgI demonstrated particularly remarkable photocatalytic performance. Notably, the photocatalyst developed in this study shows superior or at least comparable H_2O_2 production activity compared to these recently reported heterostructure systems (Table 8.2).

Table 8.2 Comparison of photocatalytic H_2O_2 generation over recently reported photocatalysts using pure water with molecular oxygen.

Photocatalysts	Reaction condition	Light Source	H_2O_2 production ($\mu mol\ h^{-1}\ g^{-1}$)	Ref.
PEI/g-C_3N_4	Water, O_2 purged	$\lambda > 420$ nm	208 $\mu mol\ h^{-1}\ g^{-1}$	[256]
$Bi_4O_5Br_2$/g-C_3N_4	Water, O_2 purged	$\lambda > 420$ nm	124 $\mu mol\ h^{-1}\ g^{-1}$	[257]
α-Fe_2O_3/CQD@g-C_3N_4	Water, O_2 purged	$\lambda > 420$ nm	138 $\mu mol\ h^{-1}\ g^{-1}$	[231]
g-C_3N_4/In_2S_3	Water, O_2 purged	$\lambda > 420$ nm	147 $\mu mol\ h^{-1}\ g^{-1}$	[258]
CdS/$K_2Ta_2O_6$	Water, O_2 purged	$\lambda > 420$ nm	346 $\mu mol\ h^{-1}\ g^{-1}$	[259]
CdS@$ZnIn_2S_4$	Water, O_2 purged	$\lambda > 420$ nm	604.8 $\mu mol\ h^{-1}\ g^{-1}$	[260]
Mn_3O_4/Co_9S_8	Water, O_2 purged	$\lambda > 420$ nm	260 $\mu mol\ h^{-1}\ g^{-1}$	[261]
$CsPbBr_3$/CTF	Water, O_2 purged	$\lambda > 420$ nm	34 $\mu mol\ h^{-1}\ g^{-1}$	[262]
2D MoS_2/$MnIn_2S_4$	Water, O_2 purged	Solar simulator	256 $\mu mol\ h^{-1}\ g^{-1}$	Chapter 3
Ag/$CuWO_4$/$NiFe_2O_4$	Water, O_2 purged	Cool white LED	930 $\mu mol\ h^{-1}\ g^{-1}$	Chapter 4
Ag/s-(Co_3O_4/$NiFe_2O_4$)	Water, O_2 purged	Cool white LED	1360 $\mu mol\ h^{-1}\ g^{-1}$	Chapter 5
10ASM	Water, O_2 purged	Cool white LED	342.3 $\mu mol\ h^{-1}\ g^{-1}$	Chapter 6
10ASM/AgI	Water, O_2 purged	Cool white LED	1473 $\mu mol\ h^{-1}\ g^{-1}$	Chapter 7

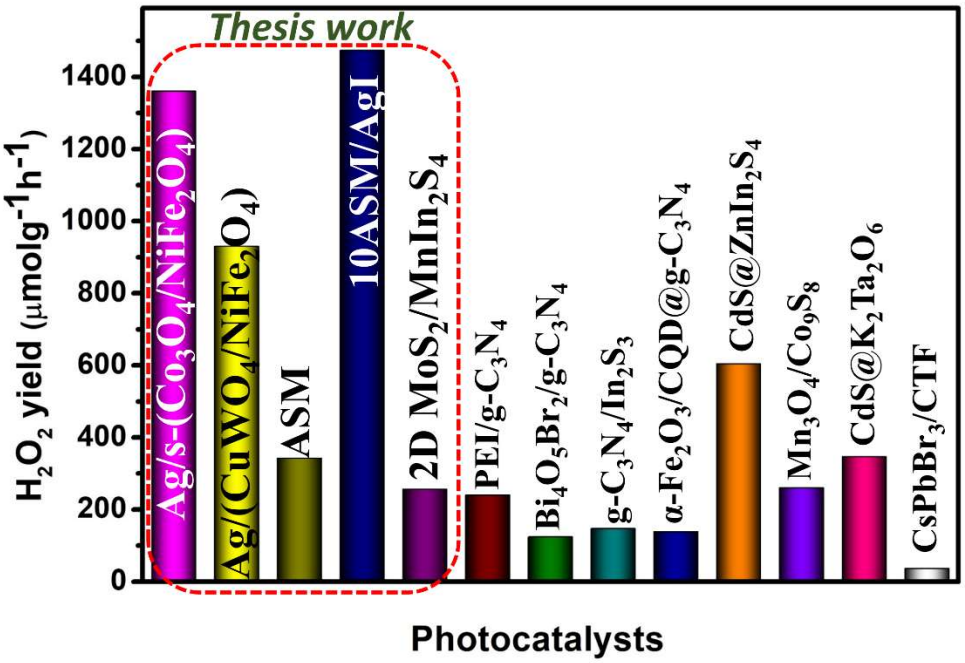

Figure 8.2. Comparison of the photocatalytic H_2O_2 production of this thesis work with recently reported photocatalysts in water with O_2 purging conditions.

This thesis emphasizes the design and development of heterostructure photocatalysts for efficient H_2O_2 production in pure water and in water under O_2-purging conditions. Achieving photocatalytic H_2O_2 generation in pure water is particularly promising for future industrial applications. Equally important is the development of photocatalysts with high recyclability and minimal performance loss, ensuring practical applicability. As shown in Figure 8.3, all the synthesized heterostructure photocatalysts maintain excellent recyclability over five consecutive cycles.

Each chapter of this thesis focused on a distinct heterostructured photocatalyst; however, the underlying improvement strategy remained consistent: maximize visible-light absorption, enhance charge separation, and ensure strong O_2/H_2O adsorption. Representative systems including 2D MoS_2/$MnIn_2S_4$, Ag/$NiFe_2O_4$/$CuWO_4$, Ag/s-(Co_3O_4/$NiFe_2O_4$), Ag loaded starch functionalized-Fe_3O_4, and Ag loaded starch functionalized-Fe_3O_4/AgI photocatalytic systems were designed with staggered band

alignments that spatially separate water oxidation and O_2 reduction processes, thereby suppressing electron–hole recombination. Several systems also exhibited Fenton-like activity, where improved H_2O_2 generation directly enhanced pollutant degradation efficiency. Looking ahead, further performance enhancement can be achieved through bandgap tuning, morphology engineering, defect modulation, and co-catalyst loading, which will simultaneously improve both H_2O_2 yield and catalyst stability.

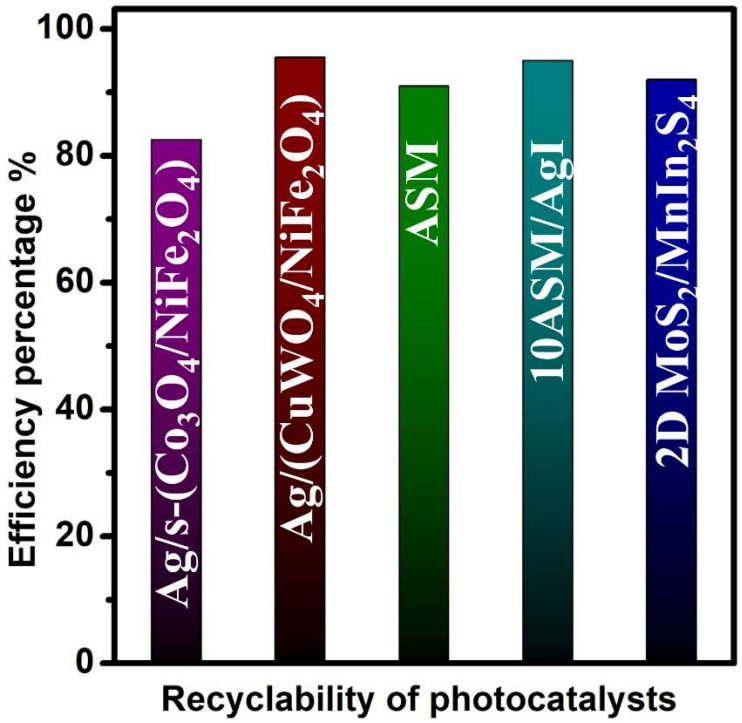

Figure 8.3. Recyclability of all the designed heterostructure photocatalysts of the present thesis work.

8.2 Future scope of this work

The future scope of this work highlights several potential directions for further research and application:

1. The as-prepared heterostructure photocatalysts, such as 2D $MoS_2/MnIn_2S_4$, $Ag/NiFe_2O_4/CuWO_4$, $Ag/s\text{-}(Co_3O_4/NiFe_2O_4)$, Ag-loaded starch-functionalized

Fe_3O_4 (ASM), and Ag-loaded starch-functionalized Fe_3O_4/AgI (10ASM/AgI), can be explored for a wide range of catalytic applications beyond H_2O_2 production.

2. During photocatalytic H_2O_2 generation, hydrogen (H_2) production may occur as a parallel reaction. Therefore, quantifying the photocatalytic H_2 evolution could provide valuable insights and should be investigated in future studies.
3. These materials hold significant potential for applications in photoelectrochemical water splitting and other electrochemical studies. Notably, in one of our recent publications, the Ag/$NiFe_2O_4$/$CuWO_4$ heterostructure demonstrated excellent electrocatalytic activity for the oxygen evolution reaction (OER). Therefore, investigating the electrocatalytic properties of the other synthesized heterostructure systems would be a promising direction for future research.
4. The synthesized heterostructures can also serve as components or supports for constructing more complex systems, such as dual Z-scheme or p-n heterojunction-based ternary composites. In one of our recent publications, we demonstrated that incorporating conductive carbon with the $NiFe_2O_4$/$CuWO_4$ system significantly enhanced OER performance. Therefore, with slight modifications, the present heterostructure systems could be adapted for various other applications in energy and environmental remediation.